ARTICLES

Self-consistent solution of Dyson's equation up to second order for atomic systems

D. Van Neck, K. Peirs,[a] and M. Waroquier
Laboratory of Theoretical Physics, Ghent University, Proeftuinstraat 86, B-9000 Gent, Belgium

(Received 28 December 2000; accepted 10 April 2001)

In this paper, the single-particle Green's function approach is applied to the atomic many-body problem. We present the self-consistent solution of the Dyson equation up to second order in the self-energy for nonrelativistic spin-compensated atoms. This Dyson second-order scheme requires the solution of the Hartree–Fock integro-differential equations as a preliminary step, which is performed in coordinate space (i.e., without an expansion in a basis set). To cope with the huge amount of poles generated in the iterative approach to tackle Dyson's equation in second order, the BAGEL (BAsis GEnerated by Lanczos) algorithm is employed. The self-consistent scheme is tested on the atomic systems He, Be, Ne, Mg, and Ar with spin-saturated ground state $^1S_0$. Predictions of the total binding energy, ionization energy, and single-particle levels are compared with those of other computational schemes [density functional theory, Hartree–Fock (HF), post-HF, and configuration interaction] and with experiment. The correlations included in the Dyson second-order algorithm produce a shift of the Hartree–Fock single-particle energies that allow for a close agreement with experiment. © *2001 American Institute of Physics.* [DOI: 10.1063/1.1376126]

I. INTRODUCTION

Over the years, the Hartree–Fock (HF) and density functional computational schemes have become quite popular in the study of atomic and molecular systems. However, the effects of electron correlation are still an intriguing issue in scientific research and subject of several studies based on various computational tools. This trend is stimulated by modern computer technology that makes feasible the study of electron correlations via advanced *first-principle* calculations. One of these first-principle methods is the Green's function formalism. Reviews on how this theory is applied in quantum chemistry are given by several authors (e.g., Refs. 1–6). This theory describes a many-body system by means of a single-particle propagator which carries all correlations resulting from the interaction with the other electrons in the atom or the molecule. The inclusion of medium effects in the construction of this so-called ''dressed'' electron propagator makes it an interesting and instructive tool to calculate in a most thorough way all ground-state properties of the electron system, such as total binding energies, ionization energies, energy levels, occupation numbers, electron charge densities, etc. The insertion of all electron correlations in the electron propagator is ensured by the introduction of an energy-dependent potential: the so-called self-energy. It is related to the Green's function by Dyson's equation, which represents an integral equation and which in principle should be solved self-consistently. The self-energy, which is in general complex and nonlocal, can be evaluated order by order in the interaction. It contains all effects of the residual two-electron interaction and is constructed with (at least in principle) exact electron propagators.

Obviously, an exact solution scheme is excluded, since it would require the solution of a fully interacting many-particle problem. However, the scheme offers a lot of opportunities to insert higher order diagrams and infinite classes of diagrams, which may not be involved in standard perturbation techniques.

The first-order approximation to Dyson's equation leads to the Hartree–Fock scheme. The corresponding Green's function, obtained by solving the Hartree–Fock equations, can be used to calculate the Hartree–Fock values of all observables of the system. This first-order approach constructs the mean field in which the electrons move but ignores electron correlation effects. To incorporate these effects in the single-particle propagator, insertion of higher order diagrams (at least of second order) in the self-energy is prerequisite.

Many attempts have been made to solve Dyson's equation up to higher order than Hartree–Fock,[3–22] but the calculations were not performed in a self-consistent way. An obvious way of obtaining an approximation for the self-energy is to employ a finite expansion for the self-energy. One example of this method is the well-known outer-valence Green's function method (OVGF),[3,8] based on the third-order expansion for the self-energy, and higher-order contributions are included by a renormalization procedure. Similar methods within this framework of third-order schemes have been worked out,[16,17,20–22] and, in particular, we mention the work of Schirmer *et al.*[7] who succeed in an algebraic diagrammatic construction (ADC) of perturbation expansions. This ADC scheme has been applied for the evaluation of one-

[a]Author to whom correspondence should be addressed; electronic mail: karel.peirs@rug.ac.be and dimitri@inwfaxp2.rug.ac.be

electron properties such like affinities, ionization energies, etc., with great success,[23,24] and references quoted therein. Holleboom *et al.*[25,26] evaluated the one-body Green's function using a second-order approximation to the self-energy that is constructed by means of the Hartree–Fock Green's function, i.e., the self-energy is not determined self-consistently. More recently, Warston *et al.*[27] applied an all-order evaluation scheme for the self-energy based on the systematic use of Dyson's integral equation. Their approach is complete up to third order in perturbation theory and large classes of higher-order effects are included in the propagator when solving Dyson's equation. However, since this scheme is not implemented self-consistently, it can not allow for the inclusion of infinite series of classes of diagrams.

All these schemes suffer from problems about the conservation of number of particles due to the lack of self-consistency. Scaling methods[23,24,28,29] have been suggested, but the physical justification of this correction is doubtful. In addition, all calculations in the above mentioned studies make use of finite basis sets. However, the loss of completeness due to the finite dimension of the basis, weakens the accuracy of the model for studying electron correlations on a highly qualitative level.

In this paper a self-consistent approach in solving the second-order Dyson equation is presented. The self-consistency ensures basic conservation laws (e.g., number of particles), but increases the computational cost considerably. In addition, the whole procedure is elaborated in an almost exact scheme: the first-order Dyson equation (corresponding to the Hartree–Fock level) is solved exactly in coordinate space, i.e., without the use of basis set functions. It implies that the Hartree–Fock eigenvalue equation, which represents a set of coupled integro-differential equations in coordinate space, is solved for each bound orbital in an iterative way on a spatial grid. To treat the continuum states in a feasible way, a discretization scheme is proposed that necessarily leads to the introduction of a basis set. However, this basis set is constructed such that the solution for the bound orbitals as obtained in coordinate space is reproduced. Using this basis set (which is complete for all practical purposes), Dyson's equation is solved up to second order in a self-consistent way. One of the main problems of solving Dyson's equation self-consistently is the huge increase of the number of poles of the Green's function after some iterations. Several suggestions have been made in the literature to cope with this phenomenon.[30–36] We apply the BAGEL (BAsis GEnerated by the Lanczos algorithm, see Refs. 30–33, 36) approach, in which the single-particle Green's function is represented in terms of a few characteristic poles, chosen in such a way as to reproduce the lowest order moments of the exact distribution.

We apply this self-consistent scheme to atomic systems. We selected a number of small atoms with closed shells (i.e., coupled to zero angular momentum) showing fully spherical symmetry and allowing for a nonrelativistic approach: He, Be, Ne, Mg, and Ar. We stress that we did not take into account screening effects higher than second order generated by ring or ladder diagrams in the self-energy. These effects can be incorporated in the self-consistent scheme but complicate substantially the proposed algorithm and are at the present stage out of the scope of this work. An extensive comparative study is presented with similar calculations at a high perturbative level and with other computational schemes (Hartree–Fock and density functional theory methods). Sufficient experimental data are available for all atoms under study to present a valuable discussion of the various computational results. In particular, special attention will be paid to the theoretical prediction of the total binding energy, ionization energies, and other single-particle energies of the electron orbitals as well as their occupation numbers.

This paper is organized as follows. In Sec. II the applied formalism and numerical scheme are outlined. Sections II A and II B are devoted to the basics of the theory and focus especially on the proper self-energy operator. The computational approach to solve the set of coupled integro-differential equations is discussed in Secs. II C, II D, and II E. In Sec. III, we present our results and give special attention to a comparative analysis between the various schemes and experiment. Finally, a summary and some conclusions are formulated in Sec. IV.

II. FORMALISM

A. The one-body Green's function

The calculations in this paper are performed using Green's function theory. In this formalism, all observables are derived from a central function, the single-particle (s.p.) propagator or one-body Green's function, that is defined in configuration and energy space as[37]

$$G_{\alpha\beta}(E)=\langle 0(A)|c_\alpha \frac{1}{E-\hat{H}+E_{0(A)}+i\eta}c_\beta^\dagger + c_\beta^\dagger \frac{1}{E+\hat{H}-E_{0(A)}-i\eta}c_\alpha|0(A)\rangle. \quad (1)$$

In this expression, the labels $\alpha,\beta,\ldots$ denote the quantum numbers of the s.p. states in a complete orthonormal basis set, $c_\alpha(c_\beta^\dagger)$ is an annihilation (creation) operator of a particle in state α (β), and η is an infinitesimal convergence parameter. Equation (1) describes the propagation of a particle or a hole in the A-electron system with Hamiltonian $\hat{H}$. The exact ground state of the A-electron system is denoted by $|0(A)\rangle$ and the corresponding energy by $E_{0(A)}$.

The second quantization form of the total Hamiltonian $\hat{H}$ reads

$$\hat{H}=\hat{H}_0+\hat{V}=\sum_{\alpha,\beta}\langle\alpha|H_0|\beta\rangle c_\alpha^\dagger c_\beta + \frac{1}{4}\sum_{\alpha,\beta,\gamma,\delta}\langle\alpha\beta|V|\gamma\delta\rangle_{as} c_\alpha^\dagger c_\beta^\dagger c_\delta c_\gamma, \quad (2)$$

where $\hat{H}_0$ contains the kinetic energy and electron-nucleus attraction, and $\langle\alpha\beta|V|\gamma\delta\rangle_{as}$ denotes an antisymmetrized matrix element of the Coulomb interaction $\hat{V}$.

From Eq. (1), the so-called Lehmann representation[37] for the Green's function is derived:

$$G_{\alpha\beta}(E)=\sum_{N(A+1)}\frac{\langle 0(A)|c_\alpha|N(A+1)\rangle\langle N(A+1)|c_\beta^\dagger|0(A)\rangle}{E-E_{N(A+1)}+E_{0(A)}+i\eta}+\sum_{N(A-1)}\frac{\langle 0(A)|c_\beta^\dagger|N(A-1)\rangle\langle N(A-1)|c_\alpha|0(A)\rangle}{E+E_{N(A-1)}-E_{0(A)}-i\eta}. \tag{3}$$

The location of the poles of the Green's function is determined by the eigenenergies $E_{N(A\pm1)}$ of the (orthonormal) eigenstates $|N(A\pm1)\rangle$ in the $(A\pm1)$-electron system, relative to the ground-state energy of the A-electron atom, i.e., by (cf. Ref. 38) the electron affinity $\mathcal{A}=E_{0(A)}-E_{N(A+1)}$ and the ionization potential $\mathcal{I}=E_{N(A-1)}-E_{0(A)}$. The residues at the poles are related to the corresponding Feynman–Dyson amplitudes[4] $\langle N(A-1)|c_\alpha|0(A)\rangle$ and $\langle 0(A)|c_\alpha|N(A+1)\rangle$. The square of these amplitudes leads to an important experimental observable namely the spectroscopic factor:

$$\begin{aligned} S_{N(A-1)}&=\sum_\alpha |\langle 0(A)|c_\alpha^\dagger|N(A-1)\rangle|^2,\\ S_{N(A+1)}&=\sum_\alpha |\langle 0(A)|c_\alpha|N(A+1)\rangle|^2. \end{aligned} \tag{4}$$

A perturbation expansion in the Coulomb interaction $\hat{V}$ can be performed for the s.p. propagator. An appropriate regrouping of the series leads to Dyson's equation for the one-body Green's function, which is expressed in matrix form as

$$[G(E)]=[G^{(0)}(E)]+[G^{(0)}(E)][\Sigma(E)][G(E)]. \tag{5}$$

In this equation, diagrammatically depicted in Fig. 1, $G^{(0)}(E)$ represents the Green's function of the noninteracting system with Hamiltonian $\hat{H}_0$, and $G(E)$ the fully-dressed Green's function of the interacting system with Hamiltonian $\hat{H}$. The (one-fermion line) irreducible self-energy, represented by $\Sigma(E)$, can be expressed as a power series in the interaction. Apart from the Coulomb interaction $\hat{V}$, each term which contributes to the series also involves a number of noninteracting propagators $G^{(0)}(E)$. Truncation of the expansion at some order in $\hat{V}$ determines the order up to which Dyson's equation is solved.

B. Self-consistent solutions of Dyson's equation

In the self-consistent Green's function formalism,[39] the internal propagators $G^{(0)}(E)$ that build the self-energy insertions should be replaced by the exact Green's function $G(E)$. Hence a solution of Dyson's equation (5) is called self-consistent if the self-energy in Eq. (5) is evaluated with the propagator $G(E)$ that coincides with the solution one tries to calculate.

This amounts to a (nonlinear) self-consistency problem, which calls for an iterative approach: starting from an initial approximation for the Green's function, the self-energy is evaluated with the s.p. propagator of the previous iteration step and is used to determine the Green's function of the present iteration. This scheme is repeated until convergence is reached, at which point a self-consistent solution is found.

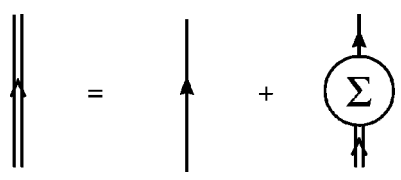

FIG. 1. Diagrammatical representation of the general Dyson equation.

The first-order self-consistent approximation to Dyson's equation leads to the Hartree–Fock (HF) equations. This is graphically represented by replacing the self-energy in Fig. 1 with its first-order approximation $\Sigma^{(1)}$ depicted in Fig. 2(a). The resulting self-energy is equal to the HF mean field, and is real and energy independent. Note that the wavy line includes a full antisymmetrization of the interaction.

The aim of the present study is to solve Dyson's equation self-consistently up to second order. This implies that the second-order contribution $\Sigma^{(2)}$, represented in Fig. 2(b), is added to the first-order self-energy $\Sigma^{(1)}$. In this case, Eq. (5) can be written as (cf. Fig. 3)

$$[G(E)]=[G^{\mathrm{HF}}(E)]+[G^{\mathrm{HF}}(E)][\Sigma^{(2)}(E)][G(E)], \tag{6}$$

where the first-order self-energy $\Sigma^{(1)}$, evaluated with $G(E)$, has been absorbed in the HF-like propagator G^{HF}, as shown in Fig. 3(b).

The analytical expression for the second-order self-energy is derived according to the Feynman rules and reads

$$\begin{aligned} \Sigma^{(2)}_{\alpha\beta}(E)=\frac{1}{(2\pi)^2}\sum_{\substack{\gamma_1,\gamma_2,\gamma_3\\ \gamma_4,\gamma_5,\gamma_6}}\frac{1}{2}\langle\alpha\gamma_6|V|\gamma_1\gamma_3\rangle_{as}\langle\gamma_2\gamma_4|V|\beta\gamma_5\rangle_{as}\\ \times\int dE_1\int dE_2\, G_{\gamma_1\gamma_2}(E-E_1+E_2)\\ \times G_{\gamma_3\gamma_4}(E_1)G_{\gamma_5\gamma_6}(E_2). \end{aligned} \tag{7}$$

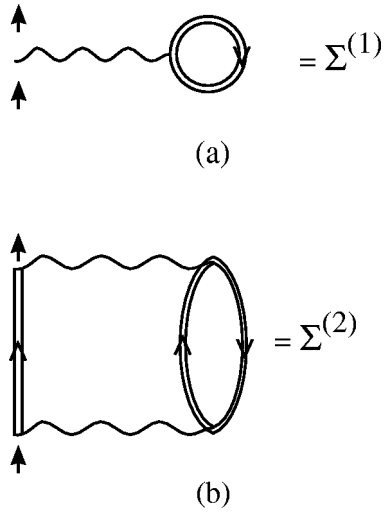

FIG. 2. Diagrammatical representation of the first-order self-energy (a) and second-order self-energy (b). Note that the antisymmetrization of the two-body interaction is systematically included in the wavy line.

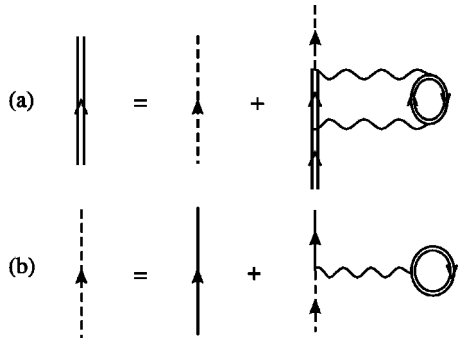

FIG. 3. Diagrammatical representation of the second-order Dyson equation.

The factor $\frac{1}{2}$ in Eq. (7) arises because of the occurrence of a pair of equivalent fermion lines in the diagram for the self-energy in Fig. 4. It perfectly compensates for the fact that some higher order diagrams are counted twice after iteration. It is noticed that the second-order contribution to the self-energy exhibits an energy dependence. The self-energy $\Sigma^{(2)}$ consists of terms that are at first sight of second order in the interaction. However, since the self-energy is to be constructed self-consistently, the s.p. propagators needed for the evaluation of $\Sigma^{(2)}_{\alpha\beta}(E)$ are those corresponding to the fully dressed Green's functions. Because their construction requires second-order diagrams as well, we easily see that the complexity of the diagrams involved in the fully dressed second-order self-energy explodes after each iteration. To gain insight in this increasing complexity, we give some examples of self-energy diagrams after one iteration in Fig. 5. We stress that the interaction represented by a wavy line in each diagram stands for the unscreened Coulomb interaction and that we do not insert polarization diagrams,[27] which describe the screened Coulomb interaction. This implies that ring diagrams of the class as shown in Fig. 6 are not involved in our self-consistent scheme. These screening diagrams are expected to incorporate long range correlations into the calculations and will be studied in a subsequent paper. We also neglect relativistic corrections as they are beyond the scope and aim of the present study. Nevertheless, for heavy atoms like Kr and Xe both screening and relativistic corrections become more and more important.[40,41] In those cases we are to be mindful when drawing conclusions.

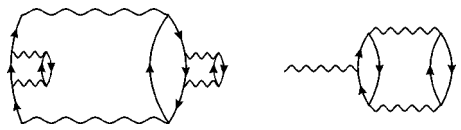

FIG. 5. Some self-energy diagrams after one iteration in the second-order Dyson equation.

C. Numerical scheme for the second-order Dyson equation

Since we will only consider closed-shell atoms, we assume spin saturation and spherical symmetry. In this case, the general s.p. indices $\alpha, \beta, \ldots$, used in the preceding sections, can be restricted to the radial quantum number and orbital angular momentum $(n_a l_a),(n_b l_b), \ldots$, in short denoted by $a,b,\ldots$. These indices are sufficient to specify a bound orbital in a nonrelativistic spherically symmetric and spin-saturated atom.

It is the intention of this study to perform the calculations as much as possible in coordinate space in order to reduce any inaccuracy due to incompleteness of the basis describing the atomic orbitals. The Dyson equation in first order, which coincides with the HF scheme, is solved exactly on a radial grid in coordinate space. In second order the self-energy diagrams contain intermediary particle and hole propagators. This implies that an electron may scatter not only to bound virtual orbitals, but also in the continuum. An exact treatment of the continuum states in coordinate space is prohibitive. Therefore, we introduce some discretization scheme of the continuum part of the HF spectrum: we add to the HF mean field a confining potential $U(r)$ of parabolic shape, starting at some distance R,

$$U(r) = C\,\theta(r-R)(r-R)^2. \tag{8}$$

Next we construct the eigenfunctions of this modified s.p. Hamiltonian, which constitute a discrete (and complete) orthonormal basis set. Finally, we truncate this set and solve the original HF problem (without the confining potential) in the so-obtained finite basis set. The resulting finite and discrete set of HF eigenfunctions is kept fixed and used throughout the subsequent calculations.

The choice of the parameters of the confining potential and the truncation of the discrete basis will be discussed in Sec. II E, but the distance R and the number of retained basis states is chosen large enough to ensure that for all occupied

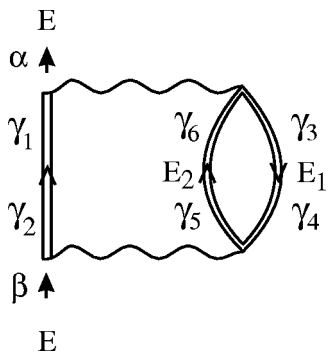

FIG. 4. Second-order self-energy.

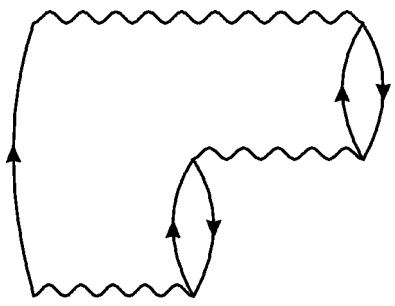

FIG. 6. A second-order ring diagram.

states the HF results in the finite basis practically coincide with the exact HF values in coordinate space.

We have assumed the s.p. propagator and self-energy to be diagonal in this basis, i.e. mixing between shells is not included. Indeed, in the case of the atoms studied here, the energy separation between orbitals that might generate a nondiagonal contribution to the Green's function is large enough to expect only a minor effect on the results. For two cases (He and Be) we have checked that the effect of including off-diagonal self-energy contributions is quite small, at least for the first iteration in the self-consistency scheme. The assumption that the self-energy matrix is diagonal in the HF basis is in principle not necessary; without this assumption, however, the numerical effort increases substantially during the iteration process to convergence.

Within this diagonal and discrete representation, the Green's function in Eq. (3) can be written as a sum of simple poles,

$$G_a(E)=\sum_j \frac{S^f_{a,j}}{E-\epsilon^f_{a,j}+i\eta}+\sum_j \frac{S^b_{a,j}}{E-\epsilon^b_{a,j}-i\eta}, \tag{9}$$

where the summation index j is restricted to the $(A\pm1)$-electron states that can be reached from the closed-shell atom by adding or removing an electron in orbital a. The first term in Eq. (9) corresponds to the so-called forward propagating part and describes excitations in the $(A+1)$-electron system, whereas the second term (backward propagating part) describes excitations in the $(A-1)$-electron system.

The second-order self-energy of Eq. (7) becomes

$$\Sigma^{(2)}_a(E)=\sum_{b,c,d}\frac{F_{ab,cd}}{4(2l_a+1)}\left\{\sum_{j,k,l}\frac{S^f_{c,j}S^f_{d,k}S^b_{b,l}}{E-(\epsilon^f_{c,j}+\epsilon^f_{d,k}-\epsilon^b_{b,l})+i\eta}+\sum_{j,k,l}\frac{S^b_{c,j}S^b_{d,k}S^f_{b,l}}{E-(\epsilon^b_{c,j}+\epsilon^b_{d,k}-\epsilon^f_{b,l})-i\eta}\right\}, \tag{10}$$

where

$$F_{ab,cd}=\sum_{LS}(2L+1)(2S+1)\left|\langle(ab)LS|V|(cd)LS\rangle_{as}\right|^2. \tag{11}$$

Because of the diagonal representation, Dyson's equation (6) can be rewritten as

$$G_a(E)=\frac{1}{E-\epsilon^{\mathrm{HF}}_a-\Sigma^{(2)}_a(E)}. \tag{12}$$

For the self-consistent solution of Dyson's equation we use the following iteration scheme. In the first iteration, the Green's function of Eq. (9) is initialized with the HF approximation,

$$G^{[1]}_a(E)=\frac{\theta(\epsilon^{\mathrm{HF}}_a-\epsilon_F)}{E-\epsilon^{\mathrm{HF}}_a+i\eta}+\frac{\theta(\epsilon_F-\epsilon^{\mathrm{HF}}_a)}{E-\epsilon^{\mathrm{HF}}_a-i\eta}. \tag{13}$$

By means of Eq. (10), the second-order self-energy in the first iteration, $\Sigma^{(2)[1]}_a$ can be found. Note that in the first iteration the S^f (S^b) coefficients are nonzero only for orbitals that are unoccupied (occupied) in the HF ground state. As a result the summation in Eq. (10) is automatically restricted to intermediate states of 2-particle 1-hole and 2-hole 1-particle nature, as in standard perturbation theory.[25]

In general, the second-order self-energy in the nth iteration, $\Sigma^{(2)[n]}_a(E)$, is evaluated, through Eq. (10), with the nth iteration Green's function $G^{[n]}_a(E)$. The Green's function $G^{[n+1]}_a(E)$ of the next iteration is then given by

$$G^{[n+1]}_a(E)=\frac{1}{E-\epsilon^{\mathrm{HF}[n]}_a-\Sigma^{(2)[n]}_a(E)},\quad n=1,2,\ldots. \tag{14}$$

In order to bring $G^{[n+1]}_a$ into the form of Eq. (9), the poles $\epsilon^{[n+1]}_{a,j}$ of $G^{[n+1]}_a$ must be found; they are the solutions of

$$\epsilon^{[n+1]}_{a,j}=\epsilon^{\mathrm{HF}[n]}_a+\Sigma^{(2)[n]}_a(\epsilon^{[n+1]}_{a,j}), \tag{15}$$

and the corresponding residues $S^{[n+1]}_{a,j}$ (the ''spectroscopic strength'' of the pole of the Green's function) are given by

$$S^{[n+1]}_{a,j}=\left(\frac{1}{1-\frac{d}{dE}\Sigma^{(2)[n]}_a(E)}\right)_{E=\epsilon^{[n+1]}_{a,j}}. \tag{16}$$

The position of the pole $\epsilon^{[n+1]}_{a,j}$ relative to the Fermi energy determines whether it should be classified as a forward or a backward contribution to Eq. (9), i.e., $\epsilon^{[n+1]}_{a,j}>\epsilon_F$ indicates an $(A+1)$ excitation and $\epsilon^{[n+1]}_{a,j}<\epsilon_F$ an $(A-1)$ excitation.

Note that the mean field $\Sigma^{(1)}$, depicted in Fig. 2(a), depends on the final Green's function. Hence after each iteration the s.p. energies ϵ^{HF} in Eq. (14) are updated to reflect the changes in the occupations of all s.p. orbitals,

$$\epsilon^{\mathrm{HF}[n]}_a=\langle a|H_0|a\rangle+\sum_{c,LS}\langle(ac)LS|V|(ac)LS\rangle_{as}\sum_j S^{b[n]}_{c,j}. \tag{17}$$

The above algorithm must be applied until convergence is reached.

D. The BAGEL approach for solving Dyson's equation

Solving Dyson's equation self-consistently within a finite discrete basis set leads to a dimensionality problem. Suppose the Green's function [Eq. (9)] of iteration n involves D poles, then it is easily seen that the corresponding second-order self-energy [Eq. (10)] has of the order of D^3 poles, and so will the Green's function in the next iteration $n+1$. Obviously, the number of poles becomes intractable quickly and numerical techniques are required to reduce this number in an acceptable way. Several methods have been proposed in the literature[30–36] and since the current study adopts the BAGEL approximation, a brief summary of this method is presented here. More details can be found in Refs. 30–33, 36.

The second-order self-energy in Eq. (10) can be written in a more compact form as

$$\Sigma^{(2)}_a(E)=\sum_{J=1}^{D^f}\frac{\sigma^f_J}{E-\omega^f_J+i\eta}+\sum_{J=1}^{D^b}\frac{\sigma^b_J}{E-\omega^b_J-i\eta}, \tag{18}$$

and contains a large number $D^f + D^b$ of simple poles. In the BAGEL(M,M) method these large sums are replaced with sums of much smaller dimension M,

$$\tilde{\Sigma}_a^{(2)}(E) = \sum_{j=1}^{M} \frac{\tilde{\sigma}_j^f}{E - \tilde{\omega}_j^f + i\eta} + \sum_{j=1}^{M} \frac{\tilde{\sigma}_j^b}{E - \tilde{\omega}_j^b - i\eta}. \tag{19}$$

The new pole energies $\tilde{\omega}_j^f$, $\tilde{\omega}_j^b$, and residues $\tilde{\sigma}_j^f$, $\tilde{\sigma}_j^b$, are determined by the requirement that the lowest energy-weighted moments of the distribution of self-energy strength are reproduced. This means that for $p = 0,1,\ldots,2M-1$,

$$m_a^f(p) = \sum_{j=1}^{M} \tilde{\sigma}_j^f (\tilde{\omega}_j^f)^p = \sum_{J=1}^{D^f} \sigma_J^f (\omega_J^f)^p, \tag{20}$$

$$m_a^b(p) = \sum_{j=1}^{M} \tilde{\sigma}_j^b (\tilde{\omega}_j^b)^p = \sum_{J=1}^{D^b} \sigma_J^b (\omega_J^b)^p. \tag{21}$$

For the construction of these new pole energies and residues, a variant of the Lanczos algorithm can be applied.

When solving Dyson's equation, the full self-energy $\Sigma_a^{(2)}(E)$ is replaced by its BAGEL(M,M) approximation $\tilde{\Sigma}_a^{(2)}(E)$. As a consequence, it can be shown that the resulting Green's function has the small number of only $2M+1$ poles, and the dimensionality during successive iterations remains fixed.

The requirements (20) and (21) on the moments of the BAGEL self-energy $\tilde{\Sigma}^{(2)}$ also restricts the distribution of spectral strength of the corresponding BAGEL Green's function: its energy-weighted moments of order $p = 0,1,\ldots,2M+1$ can be proven to equal those of the Green's function that is obtained with the original self-energy $\Sigma_a^{(2)}(E)$. Since it is required to reproduce exactly only the moments of the global strength distribution, it is not at all obvious that individual BAGEL poles of the Green's function will be close to eigenenergies of the $(A \pm 1)$-electron system. In the discussion of the results, it will become clear that BAGEL poles are spread out over a wide energy range, reproducing in this way the spectral distribution satisfactorily. The BAGEL method offers a tractable scheme to solve Dyson's equation in a self-consistent way. Once convergence has been reached, one can lift the restriction of the number of poles and also redo the calculation one iteration further within the energy bin method (see Refs. 34–36). The energy axis is discretized in a high number of energy intervals (bins). Each bin carries the summed strength of all poles belonging to that specific energy interval. This procedure allows one to get a smoother and more realistic distribution of the s.p. strength.

E. Computational parameters

As was mentioned above, the truncation of the basis set requires a careful tuning of the wall parameters to ensure a fair description of the continuum. The wall and the number of orbitals per angular momentum value of the basis set are determined on the grounds of several criteria.

(1) The HF value should have reached convergence in function of the adopted basis set. To check whether enough orbitals of high angular momentum were retained, the first iteration results (e.g., single-particle energies) of the Dyson second-order procedure are calculated for several basis sets. The final number of orbitals for each angular momentum is fixed such that this first iteration result attains convergence.

(2) The wall must not affect the HF results nor the output of the first iteration of the second-order approach and is to increase the speed of convergence.

In this way, we found that a basis set of 64 to 100 orbitals is sufficient to yield satisfactory results for the systems in the current study.

An important degree of freedom in the BAGEL approach is the number of poles M needed to describe the self-energy $\Sigma_a^{(2)}(E)$. A suitable choice of M is such that it yields a satisfactory reproduction of the strength distribution. Starting from the HF estimate as an initial guess for the s.p. Green's function for each s.p. state a, the number of poles of the self-energy in the first iteration $\Sigma_a^{(2)[1]}(E)$ is within manageable limits and the exact solution scheme (i.e., inclusion of all poles) is still tractable. However, in the next step the number of poles is roughly cubed (resulting in about 1000 poles) and at that stage, we should apply the BAGEL scheme as a tool to reduce the number of poles. In the first iteration, we are able to perform an exact calculation using the genuine poles and to compare the results with a similar calculation but applying the BAGEL poles. The number of BAGEL poles is determined such that both calculations generate the same value of the first ionization energy. For a fair agreement about 20 to 25 BAGEL poles are required.

III. RESULTS

In this section we present results of the calculations. We selected a number of small systems where Hartree–Fock is a good starting point, e.g., He and Ne. On the other hand, we chose Be and Mg as examples of atomic systems where the HF approach is known to produce less accurate results, especially in a finite-basis-set approach. We also performed calculations on heavier atomic systems such as Ar and Kr to see whether relativistic corrections are really needed to meet the experimental data.[40,41] In addition, we also include standard HF, post-HF, and DFT calculations with the GAUSSIAN 98 package[42] on the same set of atoms using a localized Gaussian basis set. The post-HF methods included electron correlations by means of different perturbation schemes such as Møller–Plesset perturbation theory (MP2, MP4) or configuration interaction (CI). An extended comparison of the numerical results of this large variety of many-body techniques is carried out and a thorough discussion of the various trends observed in the results is given. More specifically, in Sec. III A we discuss the numerical stability of the second-order Dyson results [referred to as Dyson(2)], the discretization of the continuum, and the number and the choice of the BAGEL poles. Sec. III B is devoted to a discussion of the s.p. properties (one-electron) for each atom, while Sec. III C focuses on global properties like total binding energies.

A. Numerical stability of the results

In the proposed scheme in solving the second-order Dyson equation self-consistently, the truncation of the continuum must be settled in such a way that the numerical results attain a satisfactory convergence in function of the

TABLE I. Basis sets needed for a suitable discretization of the continuum.

		He	Be	Ne	Mg	Ar	Kr
$l=0$	occ.	$1s$	$1s-2s$	$1s-2s$	$1s-3s$	$1s-3s$	$1s-4s$
	virt.	$2s-21s$	$3s-22s$	$3s-12s$	$4s-23s$	$4s-23s$	$5s-19s$
$l=1$	occ.			$2p$	$2p$	$2p-3p$	$2p-4p$
	virt.	$2p-16p$	$2p-21p$	$3p-22p$	$3p-22p$	$4p-28p$	$5p-29p$
$l=2$	occ.						$3d$
	virt.	$3d-10d$	$3d-12d$	$3d-12d$	$3d-22d$	$3d-22d$	$4d-18d$
$l=3$	occ.						
	virt.	$4f-8f$	$4f-13f$	$4f-13f$	$4f-18f$	$4f-13f$	$4f-18f$
$l=4$	occ.						
	virt.	$5g-9g$	$5g-9g$	$5g-9g$	$5g-14g$	$5g-14g$	$5g-19g$
$l=5$	occ.						
	virt.	$6h-10h$	$6h-10h$	$6h-10h$	$6h-10h$	$6h-10h$	$6h-20h$
$l=6$	occ.						
	virt.	$7i-11i$	$7i-11i$	$7i-11i$	$7i-11i$	$7i-11i$	$7i-16i$
$l=7$	occ.						
	virt.						$8j-12j$
$l=8$	occ.						
	virt.						$9k-13k$

number of continuum orbitals in the model space. This implies that the dressed Green's function (and the self-energy) remains unaffected when enlarging the basis set.

1. Discretization of the continuum

At the HF level, the one-electron orbitals and the corresponding wave functions are in first instance evaluated in coordinate space. The accuracy of these results can by no means be achieved by HF calculations using basis sets, as available in software packages. As outlined in the theoretical sections of the paper, we have to consider a lot of virtual orbitals (in the bound as well as in the continuum part of the energy spectrum), emerging as intermediate states in the higher order diagrams of the self-energy. Since an exact treatment of the continuum is unfeasible, the continuum states are discretized. We provide a method of discretization of the continuum spectrum by the insertion of a parabolic potential wall at relatively large distance from the atomic center (see Sec. II C). This discretization scheme is applied for each class of orbitals ($s,p,d,\ \ldots$ determined by the orbital momentum quantum number l). The truncation of the basis is governed by two degrees of freedom: the maximum value of the orbitals, $l_{\max}$, and the maximum number of levels, $n_{\max}$, in each class of orbitals. The choice of these discretization and truncation parameters is of the utmost importance, as it should not alter the final results.

The scheme is as follows and is repeated for each atom separately: (i) The HF equations are solved self-consistently in coordinate space without an infinite wall, yielding energies and wave functions for the occupied orbitals; (ii) the exact HF procedure is repeated including a parabolic wall with a specific curvature at some wall distance. The wall should be neither too close nor too far (avoiding too high a level density). Due to the presence of an infinite wall, all orbitals are bound levels and for each l value we are able to construct a basis set $\{\varphi_{l,i}(r)\}[i=1,\ldots,n_{\max}(l)]$. (iii) In the next step, we redo the HF calculation without wall, but within the truncated basis as constructed in (ii). The first constraint is imposed by requiring an exact reproduction of the HF results as obtained in (i). (iv) With the HF propagators determined in (iii) for both occupied and virtual orbitals, the self-energy is constructed, and the Dyson equation yields a first iteration estimate of the dressed Green's function. (v) The truncation and discretization parameters should be chosen such that the first iteration results of the Dyson equation are not altered when changing these parameters. The minimum basis sets, fulfilling these constraints are given in Table I.

The scheme proposed above turns out to be a very reliable discretization and truncation model. Repeating the whole procedure starting with other wall parameters, we succeeded in reproducing the same results, which indicates the stability, reliability and accuracy of the numerical outcome.

2. Convergence of the iterative scheme in the BAGEL approach

In the computational details (Sec. II E), it is outlined how the maximum number of BAGEL poles was established. It is found that a value of 20–25 is sufficient for gaining convergence in the reproduction of the spectral representation of the Green's function and the self-energy.

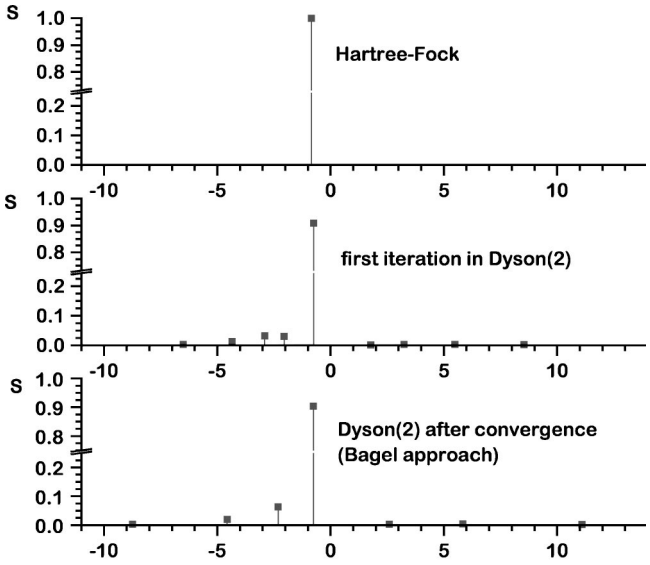

FIG. 7. Spectral function of the $2p$ orbital in Ne in Hartree–Fock [Dyson(1)] and in Dyson(2).

TABLE II. First ionization energies for some atomic systems. Dyson(1) stands for Hartree–Fock in coordinate space. Dyson(2) gives the solution of Dyson's equation in second order after one and two iterations and after convergence.

	DFT		HF		Dyson(2)			
	DFT–BLYP	DFT–B3LYP	HF/6-311g**	Dyson(1)	First it.	Second it.	Conv.	Expt.
He	0.578	0.658	0.917	0.918	0.905	0.906	0.906	0.9040[a]
Be	0.200	0.231	0.309	0.309	0.330	0.318	0.320	0.3428[b]
Ne	0.460	0.550	0.842	0.850	0.745	0.758	0.763	0.792 91[c]
Mg	0.168	0.194	0.253	0.253	0.276	0.272	0.274	0.2811[d]
Ar	0.370	0.427	0.590	0.590	0.578	0.581	0.585	0.579 46[e]
Kr	0.333	0.383	0.524	0.524	0.526	0.555	0.560	0.514 75[f]

[a]Reference 43.
[b]Reference 44.
[c]Reference 45.
[d]Reference 46.
[e]Reference 47.
[f]Reference 48.

As discussed above, the second-order Dyson equation is solved self-consistently in an iterative scheme [referred to as Dyson(2)]. In the HF approach [referred to as Dyson(1)] the spectral function,

$$S_\alpha(E)=S_p(\alpha,E)+S_h(\alpha,E), \tag{22}$$

with

$$S_p(\alpha,E)=\sum_{N(A+1)} |\langle 0(A)|c_\alpha|N(A+1)\rangle|^2 \delta(E-E_N^{(A+1)}) \tag{23}$$

and

$$S_h(\alpha,E)=\sum_{N(A-1)} |\langle 0(A)|c_\alpha^\dagger|N(A-1)\rangle|^2 \delta(E-E_N^{(A-1)}), \tag{24}$$

concentrates all strength in one peak located at the HF s.p. energy. Yet, in the plot with the first iteration (Fig. 7) a serious depletion of the strength in the HF peak is noticed. The remaining strength is distributed over $2p1h$ and $2h1p$ states.

Convergence is obtained after three to five iterations. The general trend set by the first iteration is maintained, and as a rule of thumb we notice that one pole carries about 90% of the strength. In Table II we present the first ionization energies for some atomic systems as obtained in the Dyson(2) scheme. The first column gives the exact HF estimates and some of these may differ from the experimental values in a substantial way. It is striking that the corrections resulting from the first iteration of the Dyson(2) scheme are such that experimental agreement is almost achieved, and that higher iterations until convergence have only a smooth effect on the results. Similar conclusions can be drawn concerning the total binding energies of the atomic systems (Table III). It should be stressed that the experimental agreement is surprisingly well achieved. Only a small fraction of the total ground-state energy is missing and this is probably due to additional higher order correlations not involved in Dyson(2).

TABLE III. Total ground-state energy (atomic units) obtained with various many-body models. In MP4, calculations with double–quadruple (DQ), single–double–quadruple (SDQ), and single–double–triple–quadruple (SDTQ) substitutions in the ground-state Slater determinant are considered.

		He	Be	Ne	Mg	Ar	Kr
DFT	DFT-BLYP	−2.905	−14.659	−128.940	−200.081	−527.534	−2753.748
	DFT-B3LYP	−2.913	−14.671	−128.951	−200.093	−527.553	−2753.754
HF	HF/6-311g**	−2.860	−14.572	−128.523	−199.607	−526.807	−2751.962
	Dyson(1)	−2.862	−14.573	−128.549	−199.617	−526.826	−2752.108
Post-HF	MP2	−2.885	−14.599	−128.732	−199.629	−526.954	−2752.095
	MP3	−2.889	−14.609	−128.731	−199.636	−526.966	−2752.106
	MP4(DQ)	−2.890	−14.613	−128.733	−199.638	−526.966	−2752.105
	MP4(SDQ)	−2.890	−14.613	−128.733	−199.638	−526.966	−2752.105
	MP4(SDTQ)	−2.890	−14.613	−128.736	−199.638	−526.967	−2752.107
CI	QCISD	−2.891	−14.617	−128.733	−199.635	−526.807	−2752.104
Dyson(2)	First it.	−2.899	−14.633	−128.709	−199.751	−527.075	−2751.317
	Second it.	−2.899	−14.631	−128.882	−199.944	−527.421	−2753.330
	Conv.	−2.899	−14.628	−128.888	−199.948	−527.422	−2753.243
Expt.[a]		−2.904	−14.667	−128.928	−200.043	−527.549	

[a]Reference 49.

TABLE IV. Single-particle properties. The experimental energies and occupation numbers of the valence states can be found in Refs. 53–55 for Ne, Ar, and Kr, respectively, while the energies for the core orbitals of Be and Ne are taken from Ref. 56, for Mg and Ar from Refs. 57 and 58, and for Kr from Refs. 56 and 58. The experimental energy for He is taken from Ref. 43. The Dyson(2) predictions are the results after convergence.

	Single-particle energies						Spectral strength	
	DFT–BLYP	DFT–B3LYP	HF/6-311g**	Dyson(1)	Dyson(2)	Expt.	Dyson(2)	Expt.
He 1*s*	−0.578	−0.658	−0.917	−0.918	−0.906	−0.9040	0.972	
Be 1*s*	−3.909	−4.082	−4.732	−4.733	−4.620	−4.100	0.873	
2*s*	−0.200	−0.231	−0.309	−0.309	−0.320	−0.343	0.950	
Ne 1*s*	−30.48	−30.93	−32.76	−32.77	−31.51	−31.70	0.544	
					−33.26		0.364	
2*s*	−1.298	−1.435	−1.919	−1.931	−1.750	−1.782	0.876	0.85(2)
2*p*	−0.460	−0.550	−0.842	−0.850	−0.763	−0.793	0.904	0.92(2)
Mg 1*s*	−46.24	−46.79	−49.04	−49.03	−48.20	−47.91	0.871	
2*s*	−2.906	−3.088	−3.765	−3.768	−3.815	−3.26	0.503	
					−3.399		0.442	
2*p*	−1.706	−1.833	−2.281	−2.282	−2.146	−1.81	0.882	
3*s*	−0.168	−0.194	−0.253	−0.253	−0.274	−0.2811	0.962	
Ar 1*s*	−114.3	−115.1	−118.6	−118.6	−118.0	−117.87	0.935	
2*s*	−10.83	−11.14	−12.32	−12.32	−11.93	−12.00	0.897	
2*p*	−8.459	−8.695	−9.570	−9.570	−9.519	−9.160	0.786	
3*s*	−0.875	−0.968	−1.276	−1.277	−1.159	−1.075	0.876	0.55(1)
3*p*	−0.370	−0.427	−0.590	−0.590	−0.585	−0.579	0.938	0.95(2)
Kr 1*s*	−511.0	−512.7	−520.2	−520.2	−518.6	−526.75	0.879	
2*s*	−66.43	−67.13	−69.90	−69.91	−68.67	−70.63	0.861	
2*p*	−60.12	−60.71	−63.01	−63.01	−61.87	−62.356	0.883	
3*s*	−9.334	−9.649	−10.85	−10.85	−10.14	−10.77	0.729	
3*p*	−7.090	−7.352	−8.333	−8.332	−7.756	−7.979	0.793	
3*d*	−3.058	−3.225	−3.822	−3.824	−3.566	−3.47	0.901	
4*s*	−0.807	−0.890	−1.153	−1.153	−1.119	−1.012	0.933	0.510(6)
4*p*	−0.333	−0.383	−0.524	−0.524	−0.560	−0.519	0.960	0.980(5)

B. Single-particle energies and strengths

Single-particle energies and occupation probabilities as resulting from a number of computational methods and experimental estimates are taken up in Table IV. The s.p. energies and spectral strengths of the valence shells are accessible experimentally by means of electron momentum spectroscopy (EMS). An excellent survey of this experimental technique can be found in Refs. 50–52. All experimental values given in Table IV are taken from Refs. 53–58 and compared with the theoretical predictions of various models which are fundamentally different from each other. We present HF results on two different levels: the HF/6-311g** level as the HF scheme solved with a triple-zeta polarized basis set[38] and Dyson(1) which reproduces the exact HF values as solved in coordinate space. The experiment provides the energy of orbitals designated using the total angular momentum quantum number j. To allow comparison, we made an average over the experimental levels with the same principal and angular momentum quantum number.

Apparently, use of a localized basis set does not cause significant discrepancies with the exact HF values. On the contrary, the mutual agreement is even surprisingly good, which is probably due to the particular selection of the atomic systems under study. Taking into account correlations involved in the second-order self-energy, brings the s.p. energies closer to the experimental values. Some s.p. orbitals become more bound, others evolve to a less bound pattern. The spectral strengths of the highest occupied orbitals vary from 0.90 to 0.96 in agreement with experiment. Although the correlations do become more and more important as the atomic number increases, it may be concluded that the depletion of the orbitals remains moderate on the average. This may indicate that the short-range correlations of the Coulomb force between two electrons in the atomic medium (in the presence of other electrons) are relatively weak. We notice two significant discrepancies in Table IV: the 3*s* level in Ar and the 4*s* level in Kr, where the experiment predicts a large fragmentation of the spectroscopic strength to 0.55–0.51. The failure of our theory to reproduce this particular feature is probably due to the fact that the second-order self-energy is evaluated consistent with the first order self-energy, i.e. with propagators reflecting the HF problem in the neutral atom (see Fig. 3). Some authors (e.g., Ref. 59) are able to reproduce the experimental fragmentation pattern by using the so-called ''frozen core'' s.p. energies and wave functions for the unoccupied electron orbitals. It is not clear how this can be incorporated in the framework of a self-consistent Green's function theory. For more deeply bound orbitals, we do find some substantial spreading of the spectroscopic strength. The 2*s* orbital in Mg shows two poles with almost equal strength. We applied the energy bin method to this orbital after convergence has been reached in

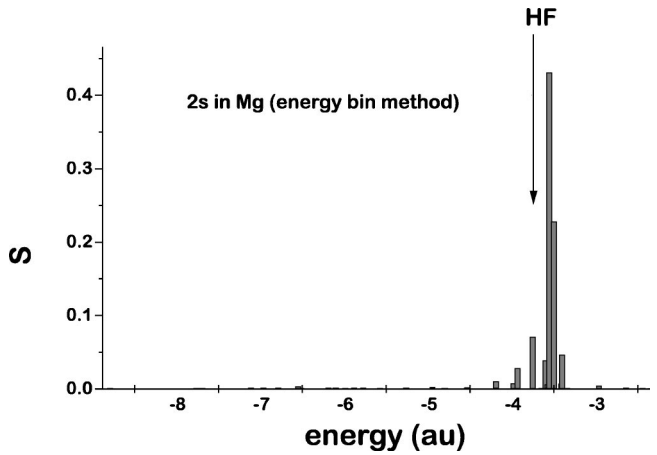

FIG. 8. Spectral function of the $2s$ orbital in Mg in Dyson(2) using the energy bin method in the last iteration.

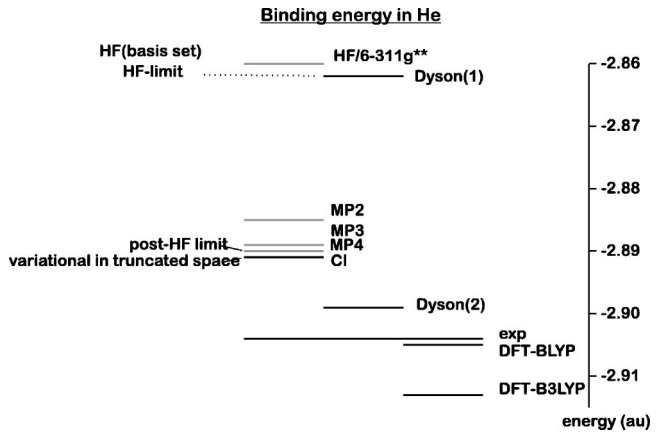

FIG. 9. Binding energies in He as obtained in various schemes. The results are separated into three classes according to the use of basis sets (HF, post-HF, CI), to the solution in coordinate space or complete basis sets [Dyson(1) and Dyson(2)] and to the use of the DFT concept.

the BAGEL approach. The spectral function is displayed in Fig. 8. In contrast to the BAGEL approach where the strength is mainly concentrated into a few poles (two poles in case of the $2s$ orbital in Mg, see Table IV), the spectral function obtained in the energy bin method presents a more realistic picture of the s.p. strength distribution. The case of Kr reveals the breakdown of the nonrelativistic approximation. Starting from the HF value, the $4s$ energy predicted in Dyson(2) approaches the experimental value in the right sense, whereas the $4p$ energy deviates from it.

C. Total binding energy

Knowledge of the dressed s.p. Green's functions for each orbital allows us to calculate the total binding energy with inclusion of all correlations implemented in Dyson(2):[37]

$$E_{gs}(A)=\frac{1}{2}\sum_{a=1}^{N_b}\frac{1}{2\pi i}\oint dE(h+E)G_a(E), \tag{25}$$

where N_b is the dimension of the basis set and h denotes the one-body part (kinetic energy and mean field) of the Hamiltonian of the system. The contour should enclose all ionization poles of the Green's function. More explicitly, this equation can be cast in the form

$$E_{gs}(A)=\frac{1}{2}\left(\langle H_0\rangle+\sum_{a=1}^{N_b}\sum_{j=1}^{M} b_{a,j}^2\epsilon_{a,j}^b\right). \tag{26}$$

Here, M is the number of backward BAGEL poles, of which $b_{a,j}^2$ represents the strength and $\epsilon_{a,j}^b$ the position. The numerical results for the atomic systems under consideration are taken up in Table III. In addition, we also take up the Hartree–Fock ground-state energies as obtained by using a localized Gaussian basis set.

The Dyson(1) prediction can be regarded as the limit of all HF results using finite basis sets (HF/6-311g** inclusive) (see Fig. 9). Perturbation schemes beyond HF involve additional correlations yielding a larger binding and achieving a better agreement with experiment. As could be expected, configuration interaction (CI) determines the limit for this class of post-HF perturbation schemes. Involving more correlations by definition Dyson(2) is obviously superior for all atomic systems under consideration, and approaches the experimental situation in a profound way. Only the DFT results can rival the Green's function method in describing the total binding energy, but these are beyond the scope of microscopic approaches due to the implementation of functionals which have an essentially empirical character. In fact, it is not surprising that the predictive power of DFT prevails on that of Dyson(2) in all cases considered here. The Becke correction[60] of the BLYP functional[61] has been determined by a least-squares fit to exact the atomic Hartree–Fock data of the six noble-gas atoms helium through radon. The B3LYP functional[62] should be regarded as an extension of the BLYP functional with exchange–correlation corrections, whose coefficients have been fitted to a high number of ionization energies, ionization potentials, proton affinities, and atomic energies. Due to the larger training set, we notice some slightly larger deviations from the experimental noble-gas data under study in this work.

IV. SUMMARY AND CONCLUSIONS

In this paper, we implemented a self-consistent approach to the Dyson equation up to second order for the atomic system. The model space was constructed such that the solution to the Hartree–Fock problem in the basis set coincides with the exact solution of the Hartree–Fock equations in coordinate space. Special care has been taken of the truncation and discretization parameters to ensure a fair description of the continuum part of the energy spectrum. The major problem remaining when solving Dyson's equation self-consistently is the enormous increase in poles over the iterations. To keep this explosion under control, the BAGEL scheme was adopted, allowing for an accurate treatment of the lowest order energy-weighted moments of the Green's function and the self-energy.

In order to test our method, we carried out extensive calculations on the ground-state configuration of the nonrelativistic closed-shell atoms He, Be, Ne, Mg, and Ar. We compared the results with other computational schemes on various levels (HF, post-HF, CI, and DFT) and with experiment. For the total energy, the ionization energy and the

single-particle levels of the atoms mentioned, the correlation incorporated in the Dyson second-order scheme produces a shift (compared to the HF results) towards the experimental value. This enables our scheme to produce an excellent prediction of these quantities, often far better than the other methods considered in this survey. We notice a distribution of the s.p. strength over complicated states over a large energy region in agreement with experiment. Only in a few cases the experimental fragmentation of the spectral strength is much larger than the theoretical estimate, but this is probably due to coincidences in the energies of some intermediate states. In the case of DFT we get a better agreement in the reproduction of the experimental total binding energies, but DFT does not belong to the family of microscopic approaches due to the empirically determined parameters in the exchange–correlation functionals. Hence its success may be attributed to undefined correlations, which are present in the employed functional but which may not be identified with some specific Feynman diagrams as in microscopic approaches such like Dyson(1) and Dyson(2). The precise relationship of the DFT formulation of many-body physics with the Green's function formalism is an intriguing and still largely unresolved issue. In the present paper, we have constructed a realistic model for the full self-energy in a series of test systems. In a subsequent study, we plan to extend the range of applicability to atoms differing from the closed-shell structure and to look into the role of long-range correlations by including screening in the interaction. The final goal of this work is to extract the density dependence of the dynamic (energy-dependent) part of the self-energy, in order to study possible energy-dependent extensions of the Kohn–Sham exchange–correlation potential.

ACKNOWLEDGMENT

This work was supported by the Fund for Scientific Research-Flanders (FWO) and the Research Board of Ghent University.

[1] J. Linderberg and Y. Öhrn, *Propagators in Quantum Chemistry* (Academic, London, 1973).
[2] Y. Öhrn, *The World of Quantum Chemistry*, edited by B. Pullman and R. Parr (Reidel, Dordrecht, 1976), p. 57.
[3] L. S. Cederbaum and W. Domcke, Adv. Chem. Phys. **36**, 205 (1977).
[4] G. Csanak, H. S. Taylor, and R. Yaris, in *Advances in Atomic and Molecular Physics*, edited by D. R. Bates and I. Esterman (Academic, New York, 1971), Vol. 7, p. 287.
[5] W. von Niessen, G. H. F. Diercksen, and L. S. Cederbaum, J. Chem. Phys. **67**, 4124 (1977).
[6] M. F. Herman, K. F. Freed, and D. L. Yeager, in *Advances in Chemical Physics*, edited by I. Prigogine and S. A. Rice (Wiley, New York, 1981), Vol. 48.
[7] J. Schirmer, L. S. Cederbaum, and O. Walter, Phys. Rev. A **28**, 1237 (1983).
[8] L. S. Cederbaum, J. Phys. B **8**, 290 (1975).
[9] L. S. Cederbaum, J. Schirmer, W. Domcke, and W. von Niessen, J. Phys. B **10**, L549 (1977).
[10] J. Schirmer, L. S. Cederbaum, W. Domcke, and W. von Niessen, Chem. Phys. **26**, 149 (1977).
[11] J. Schirmer, W. Domcke, L. S. Cederbaum, and W. von Niessen, J. Phys. B **11**, 1901 (1978).
[12] L. S. Cederbaum, W. Domcke, J. Schirmer, W. von Niessen, G. H. F. Diercksen, and W. P. Kraemer, J. Chem. Phys. **69**, 1591 (1978).
[13] J. Schirmer, L. S. Cederbaum, W. Domcke, and W. von Niessen, Chem. Phys. Lett. **57**, 582 (1978).
[14] J. Schirmer, W. Domcke, L. S. Cederbaum, W. von Niessen, and L. Asbrink, Chem. Phys. **61**, 30 (1979).
[15] W. Domcke, L. S. Cederbaum, J. Schirmer, W. von Niessen, C. E. Brion, and K. H. Tan, Chem. Phys. **40**, 171 (1979).
[16] J. Simons and W. D. Smith, J. Chem. Phys. **58**, 4899 (1973).
[17] M. F. Herman, D. L. Yeager, K. F. Freed, and V. McKoy, Chem. Phys. Lett. **46**, 1 (1977).
[18] B. T. Pickup and O. Goscinski, Mol. Phys. **26**, 1013 (1973).
[19] G. D. Purvis and Y. Öhrn, J. Chem. Phys. **60**, 4063 (1974).
[20] G. D. Purvis and Y. Öhrn, Chem. Phys. Lett. **33**, 396 (1975).
[21] P. Jørgensen and J. Simons, J. Chem. Phys. **63**, 5302 (1975).
[22] M. F. Herman, D. L. Yeager, and K. F. Freed, Chem. Phys. **29**, 77 (1978).
[23] M. S. Deleuze, M. G. Giuffreda, and J.-P. François, J. Chem. Phys. **111**, 5851 (1999).
[24] M. S. Deleuze, M. G. Giuffreda, J.-P. François, and L. S. Cederbaum, J. Phys. Chem. A **104**, 1588 (2000).
[25] L. J. Holleboom, J. G. Snijders, E. J. Baerends, and M. A. Buijse, J. Chem. Phys. **89**, 3638 (1988).
[26] L. J. Holleboom and J. G. Snijders, J. Chem. Phys. **93**, 5826 (1990).
[27] H. Warston, I. Lindgren, and S. Salomonson, Phys. Rev. A **55**, 2757 (1997).
[28] J. D. Doll and W. P. Reinhardt, J. Chem. Phys. **57**, 1169 (1972).
[29] V. Carravetta and R. Moccia, Mol. Phys. **35**, 129 (1978).
[30] H. Müther, T. Taigel, and T. T. S. Kuo, Nucl. Phys. A **482**, 601 (1988).
[31] H. Müther and L. D. Skouras, Nucl. Phys. A **555**, 541 (1993).
[32] H. Müther and L. D. Skouras, Phys. Lett. B **306**, 201 (1993).
[33] H. Müther and L. D. Skouras, Nucl. Phys. A **581**, 247 (1995).
[34] D. Van Neck, M. Waroquier, and J. Ryckebusch, Nucl. Phys. A **530**, 347 (1991).
[35] D. Van Neck, M. Waroquier, V. Van Der Sluys, and K. Heyde, Nucl. Phys. A **563**, 1 (1993).
[36] Y. Dewulf, D. Van Neck, L. Van Daele, and M. Waroquier, Phys. Lett. B **396**, 7 (1997).
[37] A. L. Fetter and J. D. Walecka, *Quantum Theory of Many Particle Systems* (McGraw-Hill, New York, 1971).
[38] A. Szabo and N. S. Ostlund, *Modern Quantum Chemistry: Introduction to Advanced Electronic Structure Theory* (McMillan, New York, 1982).
[39] R. Haussmann, *Self-consistent Quantum-Field Theory and Bosonization for Strongly Correlated Electron Systems* (Springer-Verlag, Berlin Heidelberg, 1999).
[40] L. Szasz, *The Electronic Structure of Atoms* (Wiley, New York, 1992).
[41] J. Mitroy, K. Amos, and I. Morrison, J. Phys. B **17**, 1659 (1984).
[42] M. J. Frisch, G. W. Trucks, H. B. Schlegel *et al.*, GAUSSIAN 98, Revision A.7, Gaussian, Inc., Pittsburgh, PA, 1998.
[43] S. D. Bergeson, A. Balakrishnan, K. G. H. Baldwin *et al.*, Phys. Rev. Lett. **80**, 3475 (1998).
[44] R. Beigang, D. Schmidt, and P. J. West, J. Phys. Colloq. C7 **44**, 229 (1983).
[45] K. Harth, J. Ganz, M. Raab, K. T. Lu, J. Geiger, and H. Hotop, J. Phys. B **18**, L825 (1985).
[46] V. Kaufman and W. C. Martin, J. Phys. Chem. Ref. Data **20**, 83 (1991).
[47] L. Minnhagen, J. Opt. Soc. Am. **63**, 1185 (1973).
[48] J. Sugar and A. Musgrove, J. Phys. Chem. Ref. Data **20**, 859 (1991).
[49] A. Veillard and E. Clementi, J. Chem. Phys. **49**, 2419 (1968).
[50] I. E. McCarthy and E. Weigold, Rep. Prog. Phys. **51**, 299 (1988).
[51] I. E. McCarthy and E. Weigold, Rep. Prog. Phys. **54**, 789 (1991).
[52] E. Weigold and I. E. McCarthy, *Electron Momentum Spectroscopy* (Kluwer Academic/Plenum, New York, 1999).
[53] O. Samardzic, S. W. Braidwood, E. Weigold, and M. J. Brunger, Phys. Rev. A **48**, 4390 (1993).
[54] I. E. McCarthy, R. Pascual, P. Storer, and E. Weigold, Phys. Rev. A **40**, 3041 (1989).
[55] R. Nicholson, S. W. Braidwood, I. E. McCarthy, E. Weigold, and M. J. Brunger, Phys. Rev. A **53**, 4205 (1996).
[56] J. A. Bearden and A. F. Burr, Rev. Mod. Phys. **39**, 125 (1967).
[57] J. C. Fuggle and N. Mårtensson, J. Electron Spectrosc. Relat. Phenom. **21**, 275 (1980).
[58] *Photoemission in Solids I: General Principles*, edited by M. Cardona and L. Ley (Springer-Verlag, Berlin, 1978), with additional corrections.
[59] M. Ya Amusia and A. S. Kheifets, J. Phys. B **18**, L679 (1985).
[60] A. D. Becke, Phys. Rev. A **38**, 3098 (1988).
[61] C. Lee, W. Yang, and R. G. Parr, Phys. Rev. B **37**, 785 (1988).
[62] A. D. Becke, J. Chem. Phys. **98**, 5648 (1993).